

See discussions, stats, and author profiles for this publication at: <https://www.researchgate.net/publication/247768949>

# Inversion of Pattern Anisotropy During CO Oxidation on Pt(110) Correlated with Appearance of Subsurface Oxygen

ARTICLE in THE JOURNAL OF PHYSICAL CHEMISTRY C · JANUARY 2012

Impact Factor: 4.77 · DOI: 10.1021/jp210742c

---

CITATIONS

6

---

READS

44

## 4 AUTHORS, INCLUDING:



[Christian Punckt](#)

Karlsruhe Institute of Technology

42 PUBLICATIONS 955 CITATIONS

[SEE PROFILE](#)



[Harm Hinrich Rotermund](#)

Dalhousie University

140 PUBLICATIONS 5,071 CITATIONS

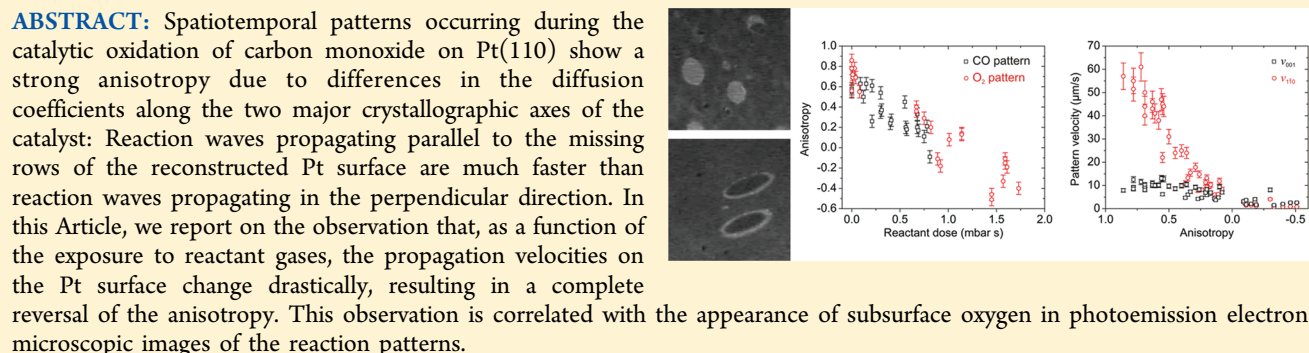
[SEE PROFILE](#)

# Inversion of Pattern Anisotropy During CO Oxidation on Pt(110) Correlated with Appearance of Subsurface Oxygen

P. Sadeghi,<sup>†</sup> K. Dunphy,<sup>†</sup> C. Punckt,<sup>‡</sup> and H. H. Rotermund\*,<sup>†</sup>

<sup>†</sup>Department of Physics and Atmospheric Science, Dalhousie University, Halifax, Nova Scotia B3H 4R2, Canada

<sup>‡</sup>Department of Chemical and Biological Engineering, Princeton University, Princeton, New Jersey 08544, United States



## INTRODUCTION

Spatiotemporal patterns arising from the complex interplay of the components of nonlinear systems far from their equilibrium are the basis of many phenomena in nature, including such diverse fields as astronomy, chemistry, and biology.<sup>1–5</sup> To gain a deeper understanding of these systems, researchers have sought more easily controllable laboratory systems that allow for a detailed study of pattern formation mechanisms.<sup>6–9</sup> One of these model systems is the catalytic oxidation of carbon monoxide on Pt(110) single crystals.<sup>10,11</sup> This heterogeneous reaction has been studied in great detail for the past few decades and was employed to demonstrate various concepts in nonlinear dynamics, ranging from basic pattern formation mechanisms<sup>12</sup> to chaos control with global<sup>13</sup> and local<sup>14,15</sup> feedback. While the physics of this reaction are generally well understood, the interplay between certain phenomena such as the formation of subsurface oxygen and the dynamics of patterns has not been fully explored. Here, we report on a newly observed phenomenon, which involves the reversal of pattern anisotropy linked to the formation of subsurface oxygen. Patterns that showed less than the expected anisotropy had been observed in the past, but were not even commented on.<sup>16</sup> Our findings indicate that the accumulation of oxygen atoms underneath the first layer of Pt atoms has a severe impact on the diffusion of adsorbed carbon monoxide molecules. Such interplay needs to be included in a comprehensive explanation of pattern formation processes in this system.

The heterogeneous catalytic oxidation of CO on Pt(110) proceeds through the Langmuir–Hinshelwood mechanism: Both reactants (CO and oxygen) have to adsorb on the surface before a reaction between neighboring adsorbate molecules can take place. Oxygen molecules dissociate during the adsorption process. Adsorbed oxygen atoms are strongly chemisorbed and,

at temperatures below 550 K, immobile. CO molecules, however, are only weakly chemisorbed and can diffuse along the Pt(110) surface.<sup>17</sup> The diffusion coefficient exhibits a strong anisotropy: along the missing rows of the reconstructed Pt surface, [1̄10] direction, the diffusion of CO molecules can be up to 3 times faster than across the missing rows.<sup>17,18</sup> Both clean and oxygen-covered Pt(110) surfaces exhibit a reconstructed surface (1 × 2 “missing row” phase). At a CO coverage greater than 0.2 ML, however, an adsorbate-induced lifting of the reconstruction to a 1 × 1 phase (bulk-truncated) sets in that is completed at a coverage of about 0.5 ML. The lifting of the reconstruction increases the oxygen sticking coefficient, which in turn gives rise to a larger reaction rate and thereby a decrease of the CO coverage.<sup>19</sup> The interplay between the reactant coverage and surface reconstruction coupled with diffusive transport of the CO gives rise to a variety of spatiotemporal patterns such as spiral waves or reaction fronts that have been observed in this system. The anisotropy in diffusion coefficients causes a strong anisotropy in these reaction-diffusion patterns (Figure 1), and the pattern anisotropy is directly related to the differences in diffusive transport along the main crystal axes. Thus, changes in the pattern anisotropy, which in this work are for the first time studied systematically for the CO oxidation system, reflect changes in the catalyst surface properties. Such changes have not been included in previous descriptions of pattern formation during the catalytic oxidation of CO.

Received: November 8, 2011

Revised: January 13, 2012

Published: January 13, 2012

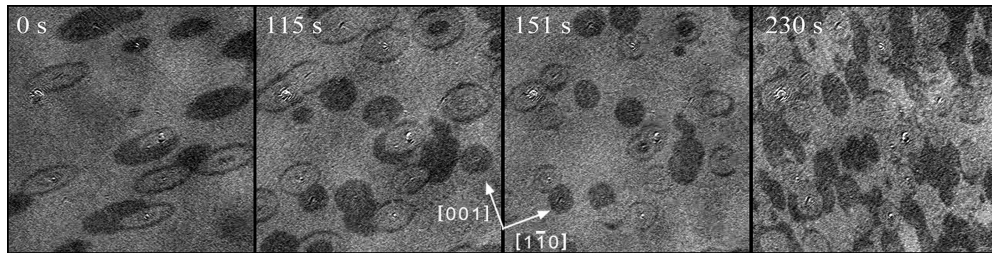


**Figure 1.** RAM pictures illustrating the change in anisotropy with time. The arrows on the picture indicate the crystal axes. The snapshots are  $500 \times 500 \mu\text{m}^2$  in size and were taken at a CO pressure range of  $(3.61\text{--}4.80) \times 10^{-4}$  mbar, an oxygen pressure range of  $(1.50\text{--}1.75) \times 10^{-3}$  mbar, and a temperature of 235 °C. The change in parameters was necessary to maintain the patterns and avoid a homogeneous surface state. Dark and light shades represent predominantly CO-covered and reactive surface areas, respectively.

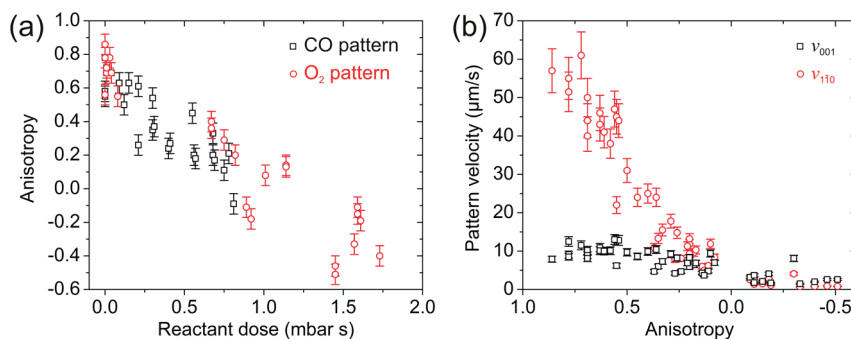


**Figure 2.** Analysis of anisotropy changes obtained in six different experiments observed with RAM at temperatures between 231 and 243 °C. (a) Anisotropy versus the total dosage of the reactant gases. Black squares correspond to CO-rich pattern on a homogeneous, predominantly oxygen-covered background, and red circles represent the opposite condition. (b) Pattern velocities as a function of anisotropy. Red circles indicate the velocity along the “fast”  $[1\bar{1}0]$  direction, while black squares represent velocities along the “slow”  $[001]$  axis.

## ■ EXPERIMENTAL METHODS

Experiments were conducted using a Pt(110) single crystal with a diameter of 10 mm, which was located inside an ultrahigh vacuum (UHV) chamber with a base pressure in the range of  $\sim 10^{-10}$  mbar. The chamber was supplied with defined partial pressures of CO and oxygen between  $10^{-5}$  mbar and atmospheric pressure employing an electronically controlled gas dosing system. The surface of the Pt(110) single crystal was cleaned prior to each experiment by repeated cycles of argon ion sputtering and annealing. Crystals were mounted on a stainless steel housing containing a standard halogen lamp, which was employed for sample heating, and the crystal temperature was monitored using two thermocouples. The crystal orientation was determined using low energy electron diffraction (LEED).

To measure changes in pattern anisotropy during CO oxidation, we studied reaction pulses and fronts that are typically observed in a temperature range of 190–280 °C and a reactant pressure range of  $10^{-5}\text{--}10^{-3}$  mbar. Under these conditions, photoemission electron microscopy (PEEM) was used as an imaging tool.<sup>20</sup> PEEM is a work function-sensitive method, which operates by mapping the number of photoelectrons that are emitted from different regions of the sample. For experiments conducted at higher pressures, reflection anisotropy microscopy (RAM) was employed, which measures the changes of the optical anisotropy of the crystal surface.<sup>21,22</sup> While RAM allows for experiments even at atmospheric pressure, it does not have the ability to identify subsurface species, which can be detected by PEEM. PEEM and RAM images were taken with a video CCD camera at a rate of 25 frames per second and stored on DVD. Further analysis of

the patterns was performed with MatLab and other image processing software.

## ■ RESULTS AND DISCUSSION

In Figure 1, we show the evolution of reaction patterns during CO oxidation imaged with RAM. Depending on reaction conditions, these patterns are CO-rich pulses and fronts, which propagate on a uniformly oxygen-covered surface or vice versa. The dark patterns in Figure 1 are formed by CO covered areas; CO adsorption lifts the  $1 \times 2$  reconstruction of the surface, and the resulting  $1 \times 1$  surface structure is less anisotropic and therefore appears dark in a RAM image. The background in Figure 1 exhibits a brighter shade due to a higher oxygen coverage which preserves the  $1 \times 2$  reconstructed state of the surface.<sup>22</sup> At an early stage of the experiment (labeled as  $t = 0$  s), target patterns and islands were elongated along the  $[1\bar{1}0]$  direction. About 2 min later, we observed isotropic patterns, and, eventually, after more than 3 min, the patterns were elongated along the  $[001]$  direction. This continuous change of pattern anisotropy initially was observed at total reactant pressures  $> 10^{-3}$  mbar. During further investigation, we found that the effect occurred also at lower reactant pressures. We therefore performed a quantitative analysis of the pattern anisotropy as a function of the reactant dosage to explore whether there was a relation between the degree of anisotropy change and the amount of reacted gas. For this purpose, we define the anisotropy  $A$  as

$$A = \log\left(\frac{v_{1\bar{1}0}}{v_{001}}\right)$$

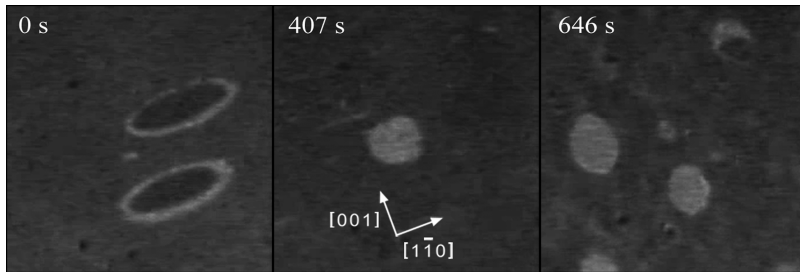


**Figure 3.** PEEM snapshots illustrating the change in crystal anisotropy. The snapshots were taken at an oxygen pressure of  $3.48 \times 10^{-4}$  mbar and a CO pressure of  $1.32 \times 10^{-4}$  mbar. The temperature drifts about 5 °C from 212 °C at the time of the first snapshot to 207 °C at the final snapshot. Each snapshot is about  $130 \times 130 \mu\text{m}^2$  in size. PEEM images work function differences; and because oxygen-covered areas have a much higher (+0.8 eV) work function than the clean surface, those areas appear dark, while CO covered areas barely increase the work function (+0.1 eV) and are imaged as light gray regions.

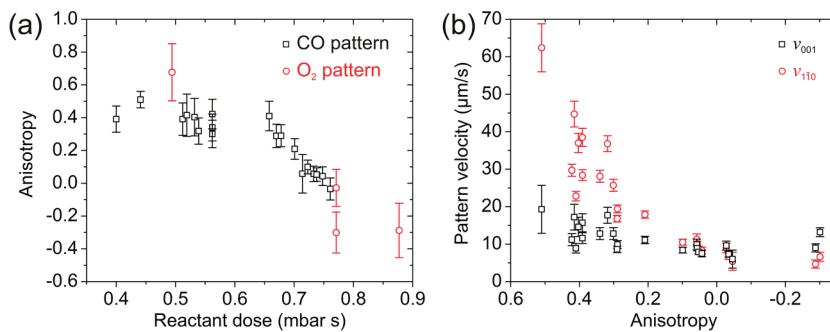


**Figure 4.** (a) Anisotropy versus the total dosage of the reactant gases obtained from one exemplary PEEM experiment. (b) Plot of pattern velocities versus the anisotropy. The experiment was performed at a mean temperature of 250 °C drifting within a  $\pm 4$  °C range at average reactant pressures of  $2.3 \times 10^{-4}$  mbar for oxygen and  $1.16 \times 10^{-4}$  mbar of CO.

where  $v$  refers to the velocity along the specified crystallographic direction.  $A > 0$  indicates pattern elongation along the “fast”  $[1\bar{1}0]$  axis,  $A = 0$  indicates a fully isotropic (circular) pattern, and  $A < 0$  represents patterns that are elongated along the “slow”  $[001]$  axis. The velocities along both crystal axes are determined from recorded image sequences by tracking reaction pulses and fronts. The RAM data are analyzed with the help of image analysis software (MatLab). Using least-squares fits of the pattern position over time, we achieve a measurement accuracy for the pattern velocities of 10% resulting in an error for the anisotropy of  $\Delta A = 0.06$  (see error bars in Figure 2). The total reactant dosage during RAM observations was calculated by integrating the preadjusted partial pressures of CO and oxygen over the duration of the experiment and was used as a rough estimate for the cumulative amount of reacted gas (see PEEM measurements below for a more precise estimate).

The data from a total of six RAM experiments are plotted in Figure 2. They were performed at temperatures between 229 and 242 °C and oxygen partial pressures (averaged over the course of the experiment) ranging from  $8.5 \times 10^{-4}$  to  $1.5 \times 10^{-3}$  mbar. We observe a clear correlation between the reactant dose and the degree of changes in pattern anisotropy (Figure 2a). Patterns initially show an anisotropy of  $A \approx 0.7$ . When a reactant dose between 0.75 and 1.0 mbar·s has been reached, patterns become isotropic, and at larger doses anisotropy inversion is observed. As can be seen in Figure 2b, the anisotropy change is the result of significant and unexpected changes in the propagation velocity of patterns along the two different crystal axes. While patterns initially propagate with velocities up to 60 μm/s in the “fast”  $[1\bar{1}0]$  direction and velocities of about 10 μm/s in the “slow”  $[001]$  direction, they

exhibit velocities of only a few μm/s when the inversion process is completed. The velocity in the originally fast direction falls below the velocity in the originally slow direction. Because the propagation of chemical waves is caused by the diffusion of CO on the Pt surface, the change in propagation velocity is a sign of profound changes in the diffusion behavior of CO molecules.

Interestingly, changes in anisotropy do not occur homogeneously across the sample. As can be seen upon closer examination of Figure 1, neighboring patterns show significant differences in aspect ratio, which are, of course, directly indicative of differences in anisotropy. Such local changes can only occur if local variations in the surface properties of the Pt crystal are present that give rise to a change in CO diffusion.

To examine the process in more detail and to obtain additional information about the chemical state of the Pt surface, we performed PEEM measurements in a much wider temperature range ( $190^\circ\text{C} < T < 280^\circ\text{C}$ ) and at various reactant pressures. This way, we were able to achieve higher spatial resolution (the resolution of RAM is about 5 μm, while PEEM can achieve submicrometer resolution). The wider temperature range was chosen to yield insight in the kinetics of the anisotropy inversion. Further, experiments performed at lower reactant pressures allowed for the use of a differentially pumped quadrupole mass spectrometer (QMS) for monitoring the amount of produced  $\text{CO}_2$  and ensuring that at the given reaction parameters the reaction rate would not drop due to surface poisoning (full coverage with CO). In the absence of surface poisoning, we can, for a given temperature, approximate the cumulative  $\text{CO}_2$  production, that is, the total amount of gas molecules reacted, by the cumulative dose of the reactants. For this purpose, we used a LabView program to accurately record the reactant partial pressures as a function of time and to

calculate the total cumulative dose of reactant gases. On the basis of QMS measurements and continuous pressure monitoring, we were able to obtain a significantly more accurate measure for the cumulative amount of reacted gas.

Figure 3 shows PEEM snapshots illustrating the changes in anisotropy during the CO oxidation reaction at smaller reactant pressures. The transformation from an anisotropic pattern to an isotropic one and eventually to an inversely anisotropic pattern occurs on a time scale of about 10 min. We first analyzed the anisotropy evolution over time for each individual experiment observed with PEEM (Figure 4) using Photoshop to determine the propagation rate of the reaction fronts. We found a behavior that corresponds well to our RAM measurements (Figure 2) regarding the degree of anisotropy change and the decrease in pattern propagation velocities. However, the reactant dosage necessary to achieve isotropic patterns (defined as  $|A| < 0.1$ ) varied strongly between experiments performed under different reaction conditions: Analyzing the complete set of data collected in a wide parameter range showed that the clear trend between reactant dose and anisotropy (seen for RAM measurements in a much narrower parameter range, Figure 2) could no longer be observed.

We hoped to obtain information about the kinetics of the process by studying the relation between the catalyst temperature and the time needed to achieve isotropic patterns: Because the reaction rate increases with increasing temperature for a Pt(110) surface in a reactive state, we expect that the required dose to achieve isotropic patterns decreases with increasing temperature. Plotting the total gas dosage versus temperature for the points when isotropy of the patterns is observed surprisingly results in a diagram that reveals no sign of a correlation between the two (Figure 5). The absence of a

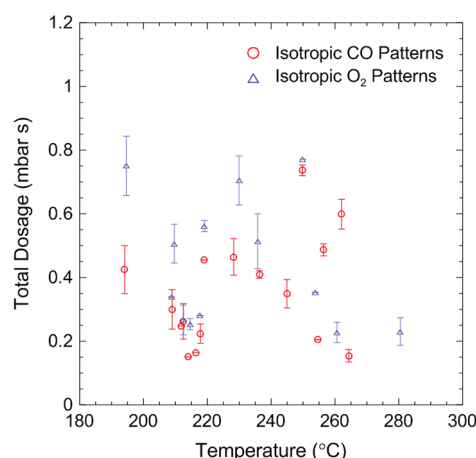


**Figure 5.** Total dosage versus the temperature for isotropic patterns. The total dosage values are scattered between 0.15 and 0.75 mbars, and no obvious correlation with temperature is observed. The temperature is the mean of the recorded values from the start of each experiment until isotropic patterns are obtained.

clear temperature correlation indicates that, although the amount of reacted gas plays a role in the inversion process, it is likely not the direct cause of the phenomenon.

We must therefore consider processes that are both related to a change in CO diffusion (being responsible for the change in propagation velocities and anisotropy) and reactant conversion (explaining the correlation with total reactant dose in RAM experiments where parameters were varied less

than in our PEEM measurement) but that also are dependent on different factors that are beyond our control, such as the exact initial state of the catalyst surface (density of atomic steps, defects).

**i. Surface Structural Changes.** Surface structural changes such as faceting can alter the diffusion behavior of adsorbed CO and thus the propagation velocities of spatiotemporal patterns. Facets form during the CO oxidation on Pt(110) and are known to mostly develop along the missing row direction of platinum.<sup>23</sup> The increasing density of facets along this originally “fast” axis of the crystal could lead to a decrease in the diffusion velocity along the missing row. On the other hand, faceting is found to be a temperature-sensitive process,<sup>24</sup> so while faceting might explain the change of anisotropy, it cannot be considered the main cause due to the lack of a temperature correlation for the change of anisotropy (Figure 5). As presented in Figure 5, even at 280 °C isotropic patterns were found, that is, at a temperature where facets are already being annealed.<sup>23</sup>

**ii. Subsurface Oxygen.** Subsurface oxygen species are oxygen atoms that have penetrated underneath the first layer of substrate atoms. Subsurface oxygen species have been observed on different surfaces such as Pd, Pt, Rh, etc.<sup>25–30</sup> These atoms lower the surface work function and are observed as bright areas in the PEEM pictures during pattern formation.<sup>31</sup> They can affect the propagation of chemical waves and can stabilize the Pt(110) surface in the nonreconstructed 1 × 1 phase.<sup>30</sup>

During our PEEM measurements, we indeed observed the occurrence of such subsurface oxygen species (see Figure 6). To elucidate their effect on the anisotropy inversion, the total reactant dose required for the observation of isotropic patterns versus the time required to perceive a noticeable sign of subsurface oxygen from the start of the experiment is plotted in Figure 6. The plot shows a clear relation between the appearance of subsurface oxygen in PEEM and the total reactant dosage at which an isotropic state is reached. Because the surface usually stays in the isotropic state for some time, the data points represent the averaged reactant dosage at which the surface is isotropic, and the associated error bars represent the duration in which isotropy was observed. However, in some experiments, examples of isotropic diffusion (patterns) are observed only for a brief period of time, so that no averaged reactant dosage or error bars can be given. One data point has been omitted in this plot. This is due to its irregular position far from the trend seen below, which is suspected to be a possible result of surface heterogeneities or preparation steps. Experiments performed at different temperature ranges (not shown) also reveal a correlation between the occurrence of subsurface oxygen and isotropic patterns. These observations suggest that the existence of subsurface oxygen may be the cause of the inversion of the pattern anisotropy. Furthermore, in previous studies of CO-oxidation on polycrystalline platinum,<sup>16</sup> spiral waves have been observed to exhibit perfectly isotropic shape, and at the same time clear patches of subsurface oxygen were found in PEEM images. This further strengthens our argument that the inversion of the anisotropy of reaction patterns is related to the formation of subsurface oxygen.

The formation of subsurface oxygen is a process that is currently not fully understood and that may depend on a variety of factors. For example, the quality of the catalyst surface is likely to play a crucial role, as the formation of subsurface species can be expected to initiate at high energy sites such as steps and defects. This may explain the absence of a direct temperature correlation, although the formation of subsurface

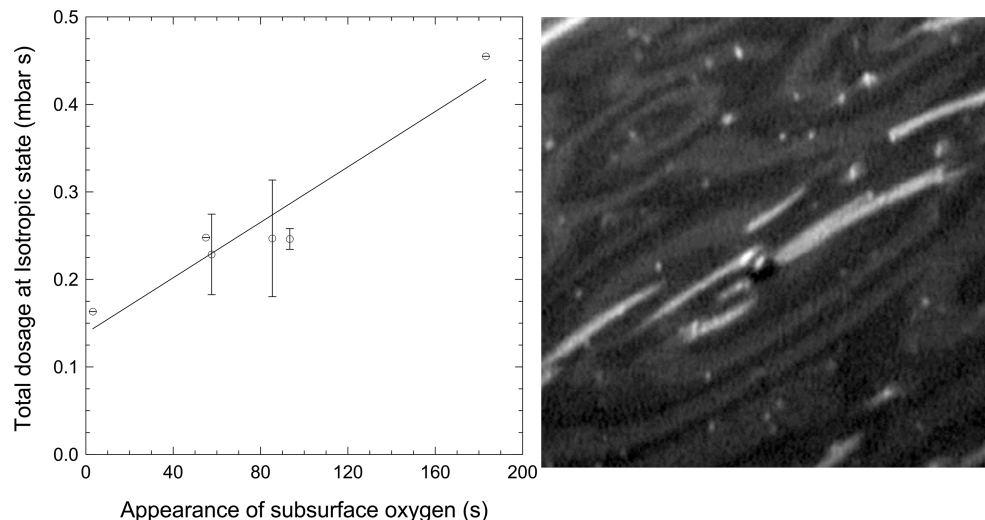


**Figure 6.** The left side plot shows the relation between the total reactant dosage at which an isotropic state is reached versus the time when the first noticeable sign of subsurface oxygen is observed. All experiments are taken in a temperature range between 208 and 219 °C and at an oxygen pressure of  $2 \times 10^{-4}$  mbar. The CO pressure is adjusted accordingly to stabilize the patterns. The error bars represent the duration in which we observe isotropy. The data points with no error bars indicate that the isotropy was observed for a very short period. On the right-hand side, a  $260 \times 260 \mu\text{m}^2$  PEEM snapshot shows subsurface oxygen as bright regions, while light and dark gray regions are associated with predominantly CO and oxygen-covered regions, respectively.

species certainly requires some degree of thermal activation. Future studies in which we systematically vary the quality of the catalyst surface may shed more light on this issue.

## CONCLUSIONS

We observed the inversion of anisotropy in spatiotemporal reaction-diffusion patterns during the catalytic oxidation of CO on Pt(110) utilizing two different surface imaging methods (RAM and PEEM). The change in anisotropy was found to depend on the total reactant dosage, and no correlation between the rate of the inversion process and the reaction temperature was observed. An analysis of experiments conducted at a constant oxygen partial pressure and within a small temperature range showed a strong correlation between the appearance of subsurface oxygen and the appearance of isotropic patterns. Until now, anisotropy of pattern formation has been attributed to the surface structure and changes of it. Here, we show that not only the two-dimensional arrangements of the surface atoms have to be taken into account to understand pattern shapes, but also the third dimension into the substrate has its own strong influence. Our discovery of a correlation between the appearance of subsurface oxygen and changes of anisotropy will open new opportunities to explain changes of anisotropy in other catalytic surface reactions.<sup>32</sup>

## AUTHOR INFORMATION

### Corresponding Author

\*E-mail: harm.rotermund@dal.ca.

### Notes

The authors declare no competing financial interest.

## ACKNOWLEDGMENTS

We would like to thank Peter Klages for his help with the image processing. We would also like to acknowledge the financial support of the Natural Sciences and Engineering Research Council of Canada (NSERC).

## REFERENCES

- (1) Falgarone, E.; Phillips, T. G.; Walker, C. K. *Astrophys. J.* **1991**, *378*, 186–201.
- (2) Fleischer, A. J.; Gauger, A.; Sedlmayr, E. *Astron. Astrophys.* **1992**, *266*, 321–339.
- (3) Bonhoeffer, K. F. *J. Gen. Physiol.* **1948**, *32*, 69–91.
- (4) Bonhoeffer, K. F. *Naturwissenschaften* **1953**, *40*, 301–311.
- (5) Winfree, A. T. *Science* **1994**, *266*, 1003–1006.
- (6) Zaikin, A. N.; Zhabotinsky, A. M. *Nature* **1970**, *225*, 535–537.
- (7) Kuhnert, L. *Nature* **1986**, *319*, 393–394.
- (8) Steinbock, O.; Toth, A.; Showalter, K. *Science* **1995**, *267*, 868–871.
- (9) Rotermund, H. H.; Engel, W.; Kordesch, M.; Ertl, G. *Nature* **1990**, *343*, 355–357.
- (10) Jakubith, S.; Rotermund, H. H.; Engel, W.; von Oertzen, A.; Ertl, G. *Phys. Rev. Lett.* **1990**, *65*, 3013–3016.
- (11) Imbihl, R. *Heterog. Chem. Rev.* **1994**, *1*, 125–133.
- (12) Nettesheim, S.; von Oertzen, A.; Rotermund, H. H.; Ertl, G. *J. Chem. Phys.* **1993**, *98*, 9977–9985.
- (13) Kim, M.; Bertram, M.; Pollmann, M.; von Oertzen, A.; Mikhailov, A. S.; Rotermund, H. H.; Ertl, G. *Science* **2001**, *292*, 1357–1360.
- (14) Wolff, J.; Papathanasiou, A. G.; Kevrekidis, I. G.; Rotermund, H. H.; Ertl, G. *Science* **2001**, *294*, 134–137.
- (15) Punckt, C.; Stich, M.; Beta, C.; Rotermund, H. H. *Phys. Rev. E* **2008**, *77*, 046222.
- (16) Lauterbach, J.; Haas, G.; Rotermund, H. H.; Ertl, G. *Surf. Sci.* **1993**, *294*, 116–130.
- (17) von Oertzen, A.; Rotermund, H. H.; Nettesheim, S. *Surf. Sci.* **1994**, *311*, 322–330.
- (18) Spiel, Ch.; Vogel, D.; Suchorski, Y.; Drachsel, W.; Schlögl, R.; Rupperechter, G. *Catal. Lett.* **2011**, *141*, 625–632.
- (19) Gritsch, T.; Coulman, D.; Behm, R. J.; Ertl, G. *Phys. Rev. Lett.* **1989**, *63*, 1086–1089.
- (20) Engel, W.; Kordesch, M. E.; Rotermund, H. H.; Kubala, S.; von Oertzen, A. *Ultramicroscopy* **1991**, *36*, 148–153.
- (21) Rotermund, H. H.; Haas, G.; Franz, R. U.; Tromp, R. M.; Ertl, G. *Science* **1995**, *270*, 608–610.
- (22) Punckt, C.; Merkt, F. S.; Rotermund, H. H. *New J. Phys.* **2007**, *9*, 213.

- (23) Monine, M. I.; Pisman, L. M.; Imbihl, R. *J. Chem. Phys.* **2004**, *121*, 11332–11344.
- (24) Ladas, S.; Imbihl, R.; Ertl, G. *Surf. Sci.* **1988**, *197*, 153–182.
- (25) Ladas, S.; Imbihl, R.; Ertl, G. *Surf. Sci.* **1989**, *219*, 88–106.
- (26) Rotermund, H. H.; Lauterbach, J.; Haas, G. *Appl. Phys. A: Mater. Sci. Process.* **1993**, *57*, 507–511.
- (27) von Oertzen, A.; Mikhailov, A.; Rotermund, H. H.; Ertl, G. *Surf. Sci.* **1996**, *350*, 259–270.
- (28) Shaikhutdinov, S. K.; Schaak, A.; Imbihl, R. *Surf. Sci.* **1997**, *391*, L1172–L1177.
- (29) Wider, J.; Greber, T.; Wetli, E.; Kreutz, T. J.; Schwaller, P.; Osterwalder, J. *Surf. Sci.* **1998**, *417*, 301–310.
- (30) von Oertzen, A.; Mikhailov, A. S.; Rotermund, H. H.; Ertl, G. *J. Phys. Chem. B* **1998**, *102*, 4966–4981.
- (31) Rotermund, H. H.; Engel, W.; Jakubith, S.; von Oertzen, A.; Ertl, G. *Ultramicroscopy* **1991**, *36*, 164–172.
- (32) Mertens, F.; Imbihl, R. *Chem. Phys. Lett.* **1995**, *242*, 221–227.